Available online at www.sciencedirect.com
ScienceDirect
Journal of Catalysis 247 (2007) 339–355
JOURNAL OF CATALYSIS
www.elsevier.com/locate/jcat

Interplay between molecular adsorption and metal–support interaction for small supported metal clusters: CO and C_2H_4 adsorption on Pd_4/γ-Al_2O_3

Manuel Corral Valero [a,b], Pascal Raybaud [b,*], Philippe Sautet [a]

[a] *Laboratoire de Chimie, Institut de Chimie de Lyon, Ecole Normale Supérieure de Lyon and CNRS, 46 Allée d'Italie, 69364 Lyon Cedex 07, France*
[b] *Direction Chimie et Physico-Chimie Appliquées, Institut Français du Pétrole, 1 & 4 Av. de Bois-Préau, 92852 Rueil-Malmaison Cedex, France*

Received 15 December 2006; revised 7 February 2007; accepted 8 February 2007

Available online 23 March 2007

Abstract

The adsorption of CO and C_2H_4 molecules was investigated on Pd_4 clusters supported on two relevant models of γ-alumina surfaces, the nonhydroxylated (100) surface and the hydroxylated (110) surface, by means of density functional theory (DFT) calculations using periodic boundary conditions. The hollow η_3 mode is the most stable geometry for CO adsorption whatever the γ-alumina surface, whereas the preferred mode for ethylene depends on the support's surface. In particular, the π mode of ethylene is stabilized when the Pd_4 cluster is deposited on the hydroxylated (110) surface. The calculations demonstrate an important interplay between molecular adsorption and cluster–oxide interaction. The deposited cluster is not a frozen object, but it responds to the molecular adsorption by relaxing its geometry and changing its bonding with the oxide support. In a counterintuitive manner, molecular adsorption on the particle reinforces its interaction with the oxide in several cases. An energy decomposition scheme is proposed to give insight into the energy trends observed. Two key energetic contributions are put forward: substrate relaxation and metal–support interaction energies. A detailed electronic analysis before and after adsorption is proposed. The combined effect of the surface ligand groups (O and Al, or OH depending on the hydration state) and of the molecular adsorbate can produce specific synergy from electronic effects between an electron donor surface O atom and an electron acceptor CO adsorbate.

Keywords: Palladium clusters; γ-Alumina; Support's effect; Metal–support interaction; CO; Ethylene (C_2H_4); Hydrogenation

1. Introduction

Interaction of molecules with metallic clusters has important implications for several applications, including heterogeneous catalysis, sensors, and magnetism [1–3]. Small metal particles offer new properties for chemistry and magnetism different from those of bulk metals, due to the presence of low-coordination atoms and electron confinement effects.

The clusters are usually stabilized by dispersion on a high-surface area solid, an oxide in most cases. Complete understanding of the microscopic processes at the interface between the metallic particle and the oxide support surface is still lacking, however, even with the great interest in the design of chemical processes on atomically well-defined supported clusters.

The main parameters to be considered on oxide-supported metal systems are the size and shape of the metal particle and the specific electronic interaction of the support. The molecular chemisorption and catalytic reactivity of Ir clusters of very small size (4 metal atoms) has been the subject of recent interesting experimental studies [4,5] revealing that the nature of the support also plays an important role in the reactivity of supported metal phases. The work of Argo et al. revealed that the hydrogenation of propylene occurs with a higher turnover frequency on Ir_4/γ-Al_2O_3 than on Ir_4/MgO [6]. Dropsch and Baerns studied the adsorption of CO on Pd supported on three different oxides (TiO_2, Al_2O_3, and SiO_2) and found more favorable CO adsorption on Pd/TiO_2 and Pd/Al_2O_3 as a result of a stronger metal–support interaction [7]. Theoretical studies of the chemisorption properties of small metallic Pd and Ni clusters on the MgO (001) surface have shown the important role of defect sites of the oxide surface [8–10]. Thus, chemical modifications of the oxide surfaces due to different pretreatment

* Corresponding author. Fax: +33 1 47 52 70 58.
E-mail address: pascal.raybaud@ifp.fr (P. Raybaud).

0021-9517/$ – see front matter
doi:10.1016/j.jcat.2007.02.014

conditions can change the metal–support interface and hence the structure and properties of the supported metal particles.

In the case of small particles, the adsorbate and support are so close that both can be considered ligands of the metal cluster. Therefore, molecular adsorption on the particle and cluster–support adhesion are two processes that might influence each other. As indicated above, it is well known that the metal–support interaction changes the adsorption properties of the particle. However, molecular adsorption on the particle also may influence the particle–support interaction. To the best of our knowledge, this latter effect has rarely been discussed in the literature.

Among the various metal–support couples, particles of Pd deposited on γ-Al_2O_3 are widely used for several catalytic applications (refining industry, car exhaust, and combustion). For refining reactions, for example, the metal phase activates C=C, C–H, and H–H bonds to increase the rates of aromatization, isomerization, and selective hydrogenation reactions. The γ-alumina and δ-alumina polymorphs are the most common supports due to their high degree of porosity and surface area (200–240 m^2/g), thus favoring a good dispersion of the active phases [11]. Moreover, the surfaces of such supports develop specific acid–base properties tuned by the addition of dopants, which contribute to the overall catalyst activity. The size distribution, morphology, and dispersion of supported metal particles depend on the preparation steps of the heterogeneous catalysts. Small metal aggregates show interesting properties for catalytic processes. Their reactivity can be controlled by the support's pretreatment process and the nature of the active-phase precursors [12,13]. Therefore, an understanding of metal–support interactions (MSI) and size effects is crucial to the design of new heterogeneous catalysts.

Many studies in the literature are devoted to alumina-supported Pd catalysts. Given the porosity and disorder of the γ-Al_2O_3 support, experimental characterization of alumina-supported heterogeneous catalysts is rather difficult. Thus, surface science experiments and theoretical studies are usually carried out on model systems, such as α-Al_2O_3 and alumina films grown on metal substrates [14–17]. Although much effort has been dedicated to this problem, extrapolating to real γ-Al_2O_3 surfaces remains difficult. Thus, density functional theory (DFT) calculations on realistic γ-Al_2O_3 models are mandatory to obtain relevant insight into heterogeneous catalysis. Carbon monoxide [18–21] and ethylene [22,23] are the most common probes for characterizing these systems. The ligands have small size in common, and thus adsorption energies are little influenced by steric effects, allowing a clear determination of the catalyst's electronic properties. Shaikhutdinov et al. [24] studied the hydrogenation of ethylene on Pd clusters supported on thin alumina films and found that the hydrogenation activity of ethylene was independent of the Pd particle size in the range of 1–3 nm. The results also demonstrate that these particles are more active than single-crystal surfaces [25]. Moreover, for large Pd particles, strongly bound di-σ ethylene was adsorbed preferentially to weakly bound π-ethylene, but this situation was reversed on small particles due to a size effect.

In the present work, we study the adsorption of these two relevant model molecules on free and γ-alumina-supported Pd_4 clusters to explore the influence of the support and the size of small metal clusters on their adsorption processes. We use a computational model of γ-Al_2O_3 that takes into account the experimental conditions for the temperature pretreatment of the support. The bulk structure of our model results from a previous DFT simulation of the topotactic transformation of boehmite into γ-Al_2O_3 [26]. One of the key findings of that study was the occupation of some nonspinel sites by Al atoms. Different theoretical approaches [27–29] led to the same result. Moreover, Digne et al. determined the variation of hydroxyl coverage as a function of temperature for the relevant (100), (110), and (111) surfaces of γ-Al_2O_3 resulting from the bulk structure of the latter [30,31]. Therefore, the influence of the support pretreatment temperature and water pressure is taken into account by the hydroxyl coverage on the surfaces of γ-alumina crystallites. During the catalyst pretreatment and activation steps, including the reduction step, the γ-alumina-supported Pd catalyst may be exposed to temperatures in the range of 200–300 °C [13]; thus, the dispersion and size distribution of the supported nanoclusters may depend both on the particle preparation steps and on the surface hydroxyl coverage [32,33]. Previous work by Corral Valero et al. [34–36] investigated the adsorption of $Pd_{n(1\leqslant n\leqslant 5)}$ clusters and Pd films on γ-alumina surfaces. These theoretical results already suggested the crucial role of hydroxylation on the stability, morphology, and wetting properties of Pd clusters on γ-alumina, an effect that must be considered to study the reactivity of the supported clusters.

In the present work, we use the γ-alumina surfaces model defined previously [30,31] to investigate the influence of metal–support interaction on the adsorption of CO and ethylene on γ-alumina-supported Pd_4 clusters that may be exposed to temperatures reaching 300 °C under normal water pressure during the preparation steps. The stable configurations of supported Pd_4 clusters used in the current work are taken directly from the previous results of Corral Valero et al. [36].

This paper is organized as follows. Section 2 presents the theoretical approach and γ-alumina models used in this work. Sections 3.1 and 3.2 are devoted to the structural and energetic analysis of CO and C_2H_4 molecules adsorbed on Pd_4 clusters (including a comparison with ideal Pd surfaces). Section 3.3 provides an electronic analysis of the metal–support interactions on these systems. Finally, Section 4 presents some conclusions.

2. Methods and models

We performed calculations at the DFT level with the Perdew–Wang [37,38] generalized gradient expansion of the exchange-correlation functional, a plane-wave basis set, and the projector augmented waves (PAW) method [39] as implemented in the Vienna ab initio simulation package (VASP) [40,41]. Calculations were carried out at the $(0.25, 0.25, 0)$ point of the reciprocal space for the reason explained previously [34,36]. The cutoff energy for all calculations is 400 eV, which ensures good convergence of the energy. The self-consistent

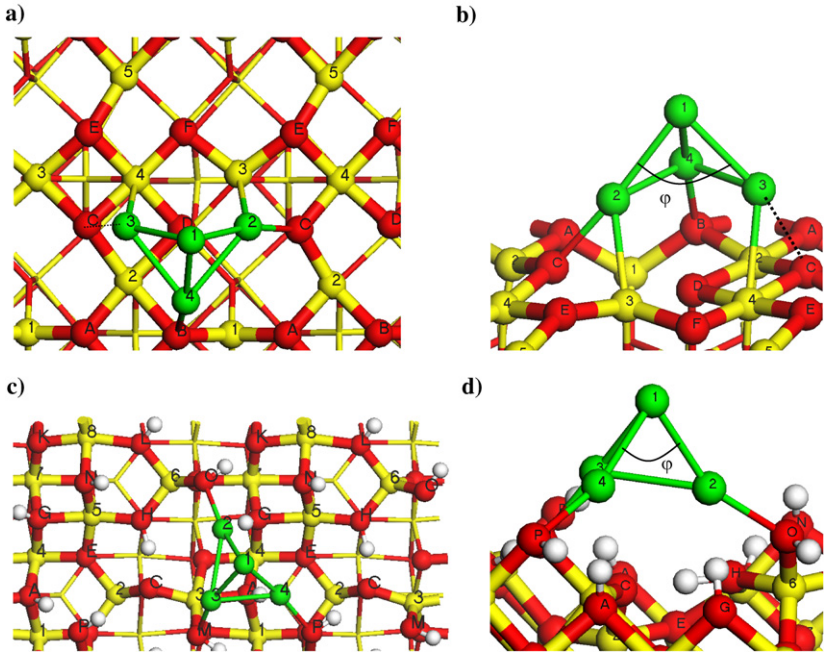

Fig. 1. Optimized structures of γ-Al_2O_3-supported Pd_4 clusters: (a) top view of the (2 × 1) unit cell of the (100) surface, (b) side view of the (100) surface, (c) top view of the (2 × 1) unit cell of the (110) surface, (d) side view of the (110) surface. (Yellow balls: Al, red balls: O, small white balls: H, green balls: Pd.) (For interpretation of the references to color in this figure legend, the reader is referred to the web version of this article.)

equations are solved with an iterative matrix diagonalization scheme (see [40]) and an energy convergence criterion of 10^{-5} eV/cycle. Geometry optimizations are performed with the conjugate-gradient algorithm and an energy convergence criterion of 10^{-4} eV/cycle.

γ-Al_2O_3 model surfaces were taken from previous work [31] considering the fact that γ-Al_2O_3 nanocrystallites exhibit two main orientations: the (100) and the (110) surfaces [11,31]. An important aspect is to use the correct degree of hydration of these surfaces. The calculations show that after pretreatment at 300 °C, the (100) surface is completely dehydrated, whereas the (110) termination, with a greater affinity with water, remains partially hydroxylated, with an estimated water coverage of 8.9 OH/nm^2, in good agreement with experimental determinations [31]. We use these two model terminations herein; their structures, along with that of an adsorbed Pd_4 cluster, are shown in Fig. 1. Our aim in the present work is to gain insight into the qualitative influence of alumina hydroxylation on the chemical properties of the adsorbed Pd_4 cluster, not to describe a specific hydroxyl coverage, which could vary on given experimental conditions. The view of the (2 × 1) supercell is shown in Fig. 1a for the (100) surface ($a = 11.14$ Å, $b = 8.39$ Å) and in Fig. 1c for the (110) ($a = 16.14$ Å, $b = 8.39$ Å). To accommodate the Pd_4 cluster with small lateral interactions between periodic images, the surface unit cell was further doubled in the y direction to obtain a (2 × 2) supercell, while the slab thickness was reduced to 4 layers to maintain reasonable computing effort [$a = 11.14$ Å and $b = 16.79$ Å for the (100) surface and $a = 16.14$ Å and $b = 16.79$ Å for the (110)]. The supercells contain 160 and 200 atoms for the (100) and hydrated (110) terminations, respectively. During geometry optimization, the two layers at the bottom of the slab were kept frozen. γ-Al_2O_3 surfaces have many nonequivalent adsorption sites; therefore, for the sake of simplicity, we use the same nomenclature as in previous work [36]; oxygen atoms are indexed with capital letters while aluminum and palladium atoms are indexed with Arabic numbers.

We considered the optimized adsorption structures for Pd_4 on these two surfaces, as described previously [36]; these are also shown in Fig. 1. For the sake of clarity, in what follows we briefly describe the structures depicted in Fig. 1 and resulting from previous work [36]. In both cases, the tetrahedron is slightly distorted with a butterfly shape, with one Pd–Pd bond elongated to about 3.2 Å. As a result, one angle (called φ) of the tetrahedron is opened from 60° to 81.6° (resp. 77.2°) on the (100) [resp. hyd(110)] surfaces. The complete structural parameters and average lengths are also reported in Tables 1 and 2 (as well as in Tables 4 and 5 for the sake of clarity) to allow direct comparisons in presence of CO and ethylene.

For the (100) dehydrated surface, three Pd–O bonds (smaller than 2.50 Å) are formed on adsorption, with an average length of 2.24 Å, corresponding to an average Pd–O coordination of 0.75. In addition, three Pd–Al bonds are formed with an average length of 2.70 Å. Because the cluster contains 4 Pd atoms, these four Pd–Al bonds correspond to a mean Pd–Al coordination number of $3/4 = 0.75$. For the (110) hydrated surface, the cluster–surface bonding scheme is different, with still three Pd–O bonds (2.17 Å), involving surface OH groups, and only one long Pd–Al interaction (3.01 Å). In this case, the Pd–Al coordination number is $\frac{1}{4}$. For both surfaces, the average Pd–Pd length is equal to 2.59 Å or 2.69 Å (depending on the largest Pd–Pd distance beyond 3.0 Å is excluded or not). Considering the slight elongation of the Pd–O and Pd–Pd bonds with respect to Ir–O and Ir–Ir bonds, our results fit reasonably well

Table 1
Interatomic distances (Å) and φ angle (°) in the optimized structures of the $CO/Pd_4/Al_2O_3(100)$ systems (see Fig. 3 for the atom labeling)

Distance/angle	η_1	η_2	η_3	Before CO ads.
C–O	1.16	1.19	1.2	1.14
Pd–C[a]	1.85	1.96/1.94	2.02/2.02/2.01	–
Pd(2)–O(C)	2.10	2.05	2.11	2.20
Pd(2)–O(D)	2.18	2.13	2.72	2.98
Pd(2)–Al(3)	2.40	2.34	2.43	2.51
Pd(3)–O(C)	2.29	2.24	2.24	2.30
Pd(3)–Al(2)	2.98	3.06	2.76	2.84
Pd(3)–Al(4)	2.58	2.89	3.04	2.66
Pd(4)–O(B)	2.19	2.24	2.30	2.23
Pd(4)–Al(2)	2.61	2.51	2.90	2.79
$\bar{d}$(Pd–O)[b]	2.19	2.17	2.22	2.24
$\bar{d}$(Pd–Al)	2.64	2.70	2.78	2.70
Pd(1)–Pd(2)	2.63	2.77	2.64	2.58
Pd(1)–Pd(3)	2.61	2.65	2.71	2.54
Pd(1)–Pd(4)	2.69	2.68	2.77	2.55
Pd(2)–Pd(3)	3.37	4.06	3.77	3.34
Pd(2)–Pd(4)	2.77	2.84	2.76	2.65
Pd(3)–Pd(4)	2.73	2.74	2.66	2.62
$\bar{d}$(Pd–Pd)[b]	2.69	2.71	2.71	2.59
φ	79.9	97.1	88.3	81.6

[a] Increasing order of the atom labeling.
[b] Average value over O-atoms (resp. Pd-atoms) at a distance smaller than 2.50 Å (2.80 Å) from Pd.

Table 2
Interatomic distances (Å) and φ angle (°) in the optimized structures of the $CO/Pd_4/Al_2O_3(110)$ systems (see Fig. 4 for the atom labeling)

Distance/angle	η_1	η_2	η_3	Before CO ads.
C–O	1.16	1.19	1.22	1.14
Pd–C[a]	1.86	1.96/1.94	2.01/1.99/1.99	–
Pd(2)–μ_1OH(O)	2.14	2.14	2.25	2.20
Pd(3)–μ_1OH(M)	2.13	2.15	2.17	2.16
Pd(4)–μ_1OH(P)	2.12	2.13	2.22	2.16
Pd(3)–Al(3)	3.08	3.00	2.88	3.01
Pd(2)–H in μ_3OH(G)	2.06	1.96	2.08	2.02
Pd(4)–H in μ_3OH(A)	2.15	2.87	2.21	2.16
$\bar{d}$(Pd–O)	2.13	2.14	2.21	2.17
Pd(1)–Pd(2)	2.55	2.62	2.71	2.54
Pd(1)–Pd(3)	2.64	2.64	2.66	2.52
Pd(1)–Pd(4)	2.64	2.61	2.75	2.55
Pd(2)-Pd(3)	2.54	2.55	2.71	2.67
Pd(2)–Pd(4)	3.67	4.29	3.02	3.22
Pd(3)–Pd(4)	2.63	2.71	2.68	2.57
$\bar{d}$(Pd–Pd)[b]	2.63	2.67	2.71	2.59
φ	89.8	110.1	67.0	78.3

[a] Increasing order of the atom labeling.
[b] Average value over Pd-atoms at a distance smaller than 2.80 Å.

with the EXAFS results obtained for Ir_4 and Rh_4 clusters on γ-Al_2O_3 [4,6]. The Pd–O coordination for distances 2.01 Å is consistently around 0.8, in good agreement with our results. In contrast, the Pd–Al coordination depends on the sample and can vary from 0.25 to 0.75. This might be related to different hydroxyl coverage in the experiment, resulting from varying preparation or pretreatment of the γ-Al_2O_3 support. In addi-

Table 3
Spin ground state, adsorption, interaction and deformation energies (eV) of gas-phase and supported Pd_4/CO complexes

	η_1	η_2	η_3
Gas-phase Pd_4			
Spin ground state	Triplet (−0.17)[a]	Singlet (−0.33)	Singlet (−1.17)
E_{ads}	−1.72	−1.88	−2.48
E_{int}	−1.74	−2.10	−2.85
$E_{def.\ substrate}$	<0.01	0.10	0.14
$E_{def.\ CO}$	0.02	0.12	0.22
Pd_4/γ-$Al_2O_3(100)$			
Spin ground state	Singlet (−0.50)	Singlet (−0.29)	Singlet (−1.00)
E_{ads}	−1.40	−2.26	−2.46
E_{int}	−2.01	−3.30	−3.21
$E_{def.\ substrate}$	0.59	0.94	0.56
$E_{def.\ CO}$	0.02	0.10	0.19
E_{MSI}[b]	−4.07	−4.78	−3.64
Pd_4/γ-$Al_2O_3(110)$			
Spin ground state	Singlet (−0.17)	Singlet (−0.68)	Singlet (−0.65)
E_{ads}	−1.65	−2.44	−2.66
E_{int}	−1.82	−3.27	−3.25
$E_{def.\ substrate}$	0.15	0.72	0.32
$E_{def.\ CO}$	0.02	0.10	0.27
E_{MSI}	−3.72	−4.25	−2.98

[a] Energy difference between the triplet and singlet spin states.
[b] The interaction energies of Pd_4 with the nonhydrated (100) and hydrated (110) surfaces before CO adsorption are −3.30 and −3.33 eV, respectively.

Table 4
Interatomic distances (Å) and relevant angles (°) of the optimized structures of $C_2H_4/Pd_4/Al_2O_3(100)$ systems (see Fig. 6 for the atom labeling)

Distance/angle	π	di-σ	Before C_2H_4 ads.
C=C	1.40	1.45	1.33
C–H[a]	1.09	1.10	1.09
θ[b]	16.15	34.12	0.0
Hybridization[b]	2.29	2.62	2.0
Pd–C[c]	2.14/2.15	2.05/2.07	–
Pd(2)–O(C)	2.16	2.22	2.20
Pd(2)–O(D)	2.31	2.53	2.98
Pd(2)–Al(3)	2.41	2.55	2.51
Pd(3)–O(C)	2.36	2.33	2.30
Pd(3)–Al(2)	2.92	2.52	2.84
Pd(3)–Al(4)	2.59	2.76	2.66
Pd(4)–O(B)	2.20	2.17	2.23
Pd(4)–Al(2)	2.77	2.95	2.79
$\bar{d}$(Pd–O)[d]	2.26	2.31	2.24
$\bar{d}$(Pd–Al)	2.67	2.70	2.70
Pd(1)–Pd(2)	2.61	2.63	2.58
Pd(1)–Pd(3)	2.61	2.63	2.54
Pd(1)–Pd(4)	2.67	2.62	2.55
Pd(2)–Pd(3)	3.07	3.22	3.34
Pd(2)–Pd(4)	2.74	2.72	2.65
Pd(3)–Pd(4)	2.71	2.64	2.62
$\bar{d}$(Pd–Pd)	2.67	2.65	2.59
φ	72.1	75.5	81.6

[a] Average C–H bond lengths considered.
[b] See text for definition.
[c] Increasing order of the atom labeling.
[d] Average value over O-atoms (Pd-atoms) at a distance smaller than 2.50 Å (2.80 Å) from Pd.

Table 5
Interatomic distances (Å) and relevant angles (°) of the optimized structures of $C_2H_4/Pd_4/Al_2O_3(110)$ systems (see Fig. 7 for the atom labeling)

Distance/angle	π	di-σ	Before C_2H_4 ads.
C=C	1.40	1.46	1.33
C–H[a]	1.09	1.10	1.09
θ[b]	16.29	36.39	0
Hybridization[b]	2.30	2.66	2.00
Pd–C[c]	2.13/2.14	2.04/2.05	–
Pd(2)–μ_1OH(O)	2.21	2.31	2.20
Pd(3)–μ_1OH(M)	2.10	2.11	2.16
Pd(4)–μ_1OH(P)	2.25	2.17	2.16
Pd(3)–Al(3)	3.18	3.00	3.01
Pd(2)–H in μ_3OH(G)	2.04	2.29	2.02
Pd(4)–H in μ_3OH(A)	1.89	2.01	2.16
$\bar{d}$(Pd–O)	2.19	2.20	2.17
Pd(1)–Pd(2)	2.70	2.64	2.54
Pd(1)–Pd(3)	2.54	2.63	2.52
Pd(1)–Pd(4)	2.70	2.63	2.55
Pd(2)–Pd(3)	2.57	2.64	2.67
Pd(2)–Pd(4)	2.84	2.95	3.22
Pd(3)–Pd(4)	2.61	2.68	2.57
$\bar{d}$(Pd–Pd)[d]	2.62	2.64	2.57
φ	63.5	68.1	78.3

[a] Average C–H bond lengths considered.
[b] See text for definition.
[c] Increasing order of the atom labeling.
[d] Average value over Pd-atoms at a distance smaller than 2.80 Å.

tion, it is well known that the metal–Al contributions are determined with far less confidence in EXAFS and can be screened by metal–O contributions.

CO and C_2H_4 molecules were adsorbed on all nonequivalent positions of the supported metal cluster. We report only the structures with the most stable adsorption energies, calculated as

$$E_{\text{ads}}(\text{X}) = E(\text{X–Pd}_4/\gamma\text{-Al}_2\text{O}_3) - E(\text{X}) - E(\text{Pd}_4/\gamma\text{-Al}_2\text{O}_3), \tag{1}$$

where X is either CO or C_2H_4. We decompose the adsorption energy into deformation and interaction energy contributions to analyze the chemisorption process. During this process, the two partners (molecule and substrate, defined as alumina surface plus Pd_4 cluster) are deformed with respect to their separated equilibrium geometries. Distorting the substrate or molecule alone toward the geometry that it adopts in the chemisorption complex requires some energy, defined as the substrate or molecule deformation energy. For the substrate, this deformation energy is calculated as

$$E_{\text{def. substrate}} = E(\text{Pd}_4/\gamma\text{-Al}_2\text{O}_3') - E(\text{Pd}_4/\gamma\text{-Al}_2\text{O}_3), \tag{2}$$

where $E(\text{Pd}_4/\gamma\text{-Al}_2\text{O}_3')$ is the energy of the substrate with the deformed geometry obtained after CO or C_2H_4 adsorption. This deformation energy clearly depends on the adsorbate. Deformation energies for CO or C_2H_4 molecules are calculated in a similar way.

The interaction energy is defined as the binding energy between the substrate and the molecule, keeping each partner frozen in the deformed geometry adopted in the chemisorption complex,

$$E_{\text{int}}(\text{X}) = E(\text{X–Pd}_4/\gamma\text{-Al}_2\text{O}_3) - E(\text{X}') - E(\text{Pd}_4/\gamma\text{-Al}_2\text{O}_3'). \tag{3}$$

Thus, the adsorption energy can be decomposed according to:

$$E_{\text{ads}} = E_{\text{int}} + E_{\text{def. substrate}} + E_{\text{def. molecule}}. \tag{4}$$

This energy decomposition scheme clearly shows that adsorption energies are a trade-off between two antagonistic effects: interaction and deformation energies. Interaction energies are exothermic, which clearly shows that the metal to adsorbate bond formation is the driving force of the chemisorption process. However, some of the energy obtained by the new bonds between the metal and the incoming ligand is spent by the electronic and geometrical rearrangement accounted for by the endothermic deformation energies.

The interaction between the cluster and the oxide surface is another key parameter. Metal–support interaction energies, E_{MSI}, are computed as the energy difference between the slab with the cluster and chemisorbed molecule, minus that of the oxide surface and that of the isolated X–Pd_4 fragment. In other words, the cluster–support interaction is broken, all partners are kept in the deformed geometry of the X–Pd_4/γ-Al_2O_3 system. Thus,

$$E_{\text{MSI}}(\text{X}) = E(\text{X–Pd}_4/\gamma\text{-Al}_2\text{O}_3) - E(\text{X–Pd}_4') - E(\gamma\text{-Al}_2\text{O}_3'). \tag{5}$$

The E_{MSI} parameter can be used as a measure of the change in the electronic structure at the metal–support interface induced by the adsorption of the probe molecules.

A careful investigation of the magnetic ground state has been carried out both for the isolated Pd_4 ligand and for the γ-alumina supported surfaces. For the gas-phase Pd_4 cluster, it is known that the triplet spin state is the most stable configuration [36,42,43] and it will be chosen as the reference state for adsorption energies. For the Pd_4 cluster supported on the (100) and (110) γ-alumina surface, we found that the magnetic ground state remains the triplet state (also chosen as the reference) even though the difference in energy with the low spin state is small. The magnetic ground state of other systems are reported in Tables 3 and 6 and are discussed in Section 3.

Finally, the electronic analysis implying density of states (DOS) diagrams with spin projection (when necessary) are calculated and presented in Section 3.3.

3. Results and discussion

3.1. Adsorption of carbon monoxide: Structure and energies

The structure of CO molecules adsorbed on isolated Pd_4 clusters and Pd_4 supported on the (100) surface and on the hydrated (110) surface of γ-Al_2O_3 are presented in Figs. 2–4. The relevant interatomic distances in supported Pd_4 are reported in Tables 1 and 2. Table 3 summarizes the relevant energy contributions and electronic ground state for these systems. Although

Table 6
Spin ground state, adsorption, interaction and deformation energies (eV) and hybridization indexes of C_2H_4/Pd_4 complexes

	π	di-σ
Gas-phase Pd_4		
Spin ground state	Triplet (−0.18)[a]	Triplet (−0.22)
E_{ads}	−1.22	−0.89
E_{int}	−1.43	−1.72
$E_{def.\ substrate}$	<0.01	<0.01
$E_{def.\ ethene}$	0.21	0.83
Pd_4/γ-Al_2O_3(100)		
Spin ground state	Singlet (−0.10)	Singlet (−0.37)
E_{ads}	−0.75	−0.88
E_{int}	−1.38	−2.28
$E_{def.\ substrate}$	0.38	0.40
$E_{def.\ ethene}$	0.26	1.00
E_{MSI}[b]	−3.49	−2.97
Pd_4/γ-Al_2O_3(110)		
Spin ground state	Singlet (−0.09)	Singlet (−0.17)
E_{ads}	−1.09	−0.99
E_{int}	−1.59	−2.18
$E_{def.\ substrate}$	0.22	0.19
$E_{def.\ ethene}$	0.27	1.00
E_{MSI}	−3.12	−2.86

[a] Energy difference between the triplet and singlet spin state.
[b] The interaction energy of Pd_4 with the nonhydrated (100) and hydrated (110) surfaces before ethene adsorption is −3.30 and −3.33 eV, respectively.

the molecule can occupy various nonequivalent positions (top, bridge, and hollow sites) on the supported cluster, only the most stable situation is shown. Among the configurations tested, we have also investigated the case where the CO molecule is initially located with C linked to Pd atoms while the O atom interacts with one Al atom of the (100) surface. However, this configuration (not represented here) is not stable and CO relaxes in a position where O no longer interacts with the support. This result shows that a dual adsorption mode for CO both on the particle and on the support is not possible, favoring an interaction with the Pd atoms only.

3.1.1. Structural analysis

An analysis of the results reported in Tables 1 and 2 and Figs. 2–4, reveals the structural trends as the coordination of the CO molecule with a given substrate increases. For gas-phase clusters and supported systems, the Pd–CO bond lengthens with increased CO coordination due to a bond order conservation mechanism. This effect is in line with the increase of Pd–Pd bond distances of these systems after CO adsorption, especially for the metal atoms coordinated to the ligand. The CO bond elongation along one row is known to result from the enhancement of backbonding effects from metal to ligand with increasing Pd–CO coordination [44]. Therefore, these general well-known trends for ideal metal surfaces are recovered for the Pd_4 cluster studied here.

We now focus on the different optimized structures obtained on the (100) and hydrated (110) surfaces. The former surface exhibits a strong rearrangement of both the oxide support and

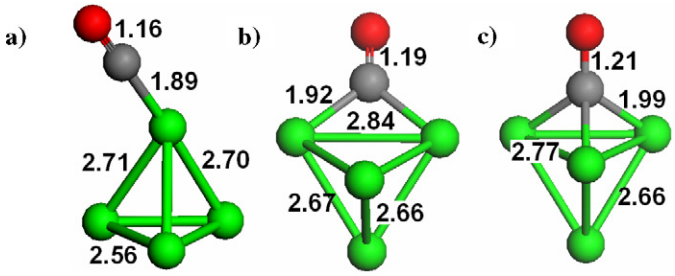

Fig. 2. Optimized structures (distances in Å) of the gas-phase CO/Pd_4 complexes: (a) η_1 (top), (b) η_2 (bridge), (c) η_3 (hollow). (Green balls: Pd, gray balls: C, red balls: O.) (For interpretation of the references to color in this figure legend, the reader is referred to the web version of this article.)

the Pd tetramer after CO adsorption. The φ angle in Figs. 3 and 4 can be considered as a measure of metal aggregate deformation. Large bond angles are associated with flat Pd_4 clusters strongly interacting with the surface. Its value clearly shows that the Pd_4 cluster has a flatter structure, especially for the η_2 coordination. At the same time, average Pd–Pd distances for supported clusters are strongly elongated compared with those in isolated CO/Pd_4 systems. A first analysis in terms of distances can be obtained on the influence of CO chemisorption on the cluster–oxide surface interaction. Based on a bond-order conservation principle, the Pd atoms directly bound to the CO molecule are expected to have a weaker interaction with the substrate, whereas those not bound to the CO develop a weaker interaction with the other Pd atoms (bound directly to CO), and hence indirectly strengthen their interaction with the surface. Although this is verified in several cases, especially for the Pd–Al bonds, it is not a general property. Indeed, surprisingly, the interaction between Pd and oxygen surface atoms is globally strengthened on CO adsorption with a marked shortening of the Pd(2)–O(C) distance and the creation of a new Pd(2)–O(D) bond [Pd(2) is not bound to CO] but also a shortening of Pd(3)–O(C) for the η_2 chemisorption mode [where Pd(3) is bound to CO]. The local coordination of the Pd(2) atom after such a Pd–surface bond contraction is similar to that found in strongly interacting Pd clusters, such as Pd monomers at low metal coverage, Pd dimmers, and linear Pd trimers (see [36] for details). Pd–surface bond contractions are less pronounced for the η_3 coordination.

For the hydrated (110) surface, variations of CO, Pd–C, and Pd–Pd bond lengths are similar; however the influence of CO adsorption on the particle–oxide interface is completely different. Indeed, no new Pd–O bond is created, and the Pd–OH bonds are only slightly shorter (−0.01 to −0.06 Å) after CO adsorption in η_1 and η_2 modes. In contrast, Pd–OH bonds are elongated after CO adsorption in the η_3 mode. Along these same lines, the distortion of the supported Pd_4 cluster, measured by the φ angle, is even smaller in this case than before CO adsorption. The average Pd–O distance is also slightly increased in the η_3 mode. From this analysis, it appears that on the hydrated (110) Al_2O_3 surface, the structure of the Pd_4 cluster does not exhibit such a strong rearrangement after CO adsorption as that observed for the dehydrated γ-Al_2O_3(100) system. The following energetic analysis supports this behavior.

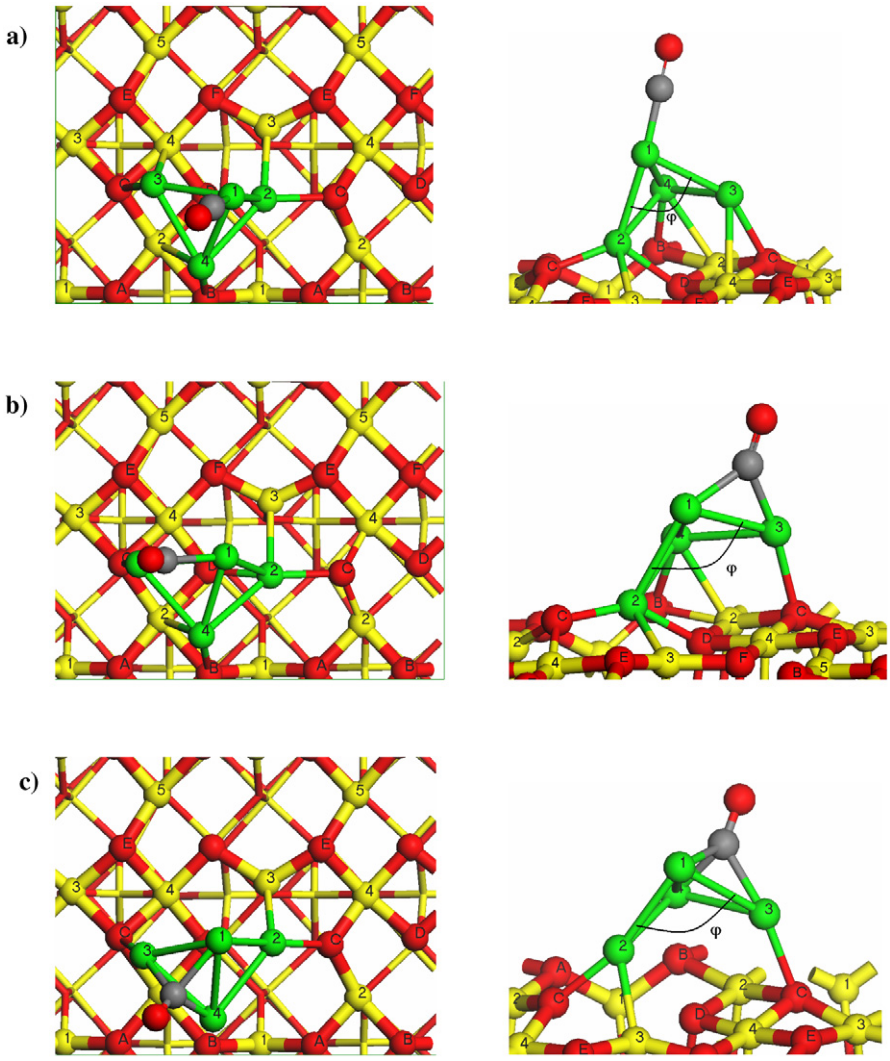

Fig. 3. Top view (left) and side view (right) of the (2 × 1) unit cell of the optimized structures of the CO/Pd_4/Al_2O_3(100) systems: (a) η_1 (top), (b) η_2 (bridge), (c) η_3 (hollow). (Yellow balls: Al, red balls: O, green balls: Pd, gray balls: C.) (For interpretation of the references to color in this figure legend, the reader is referred to the web version of this article.)

3.1.2. Energetic analysis

According to results reported in Table 3, the comparison of CO adsorption energies on isolated Pd_4 clusters with adsorption energies on supported clusters reveals first that the adsorption energies on Pd_4 are strongly favored with respect to the adsorption on the support surfaces. Indeed, comparing previous DFT adsorption energies of CO on the same γ-alumina surfaces [31] shows that the adsorption energies are significantly more exothermic on the Pd_4 clusters (whatever the mode) than on the support Al sites with low coordination number. Previously [31], the adsorption energies were calculated as −0.21 to −0.41 eV for the Al_V sites of the (100) surface, and the maximum adsorption energy (−0.79 eV) was found for the Al_{III} site of the (110) surface. These values are thus 3–10 times smaller than the adsorption energies on the supported Pd_4 clusters. As previously explained, simultaneous interactions of CO with one Al atom of the support and Pd atoms are also ruled out by our calculations. These results clearly imply that small pulses of CO molecules will preferentially probe the metallic sites of the Pd_4 clusters.

According to Table 3, the γ-Al_2O_3 support strengthens the η_2 mode by 0.4–0.6 eV; however, it remains less favorable than the η_3 mode, for which only a small change in the adsorption energy (up to +0.18 eV) is observed with respect to the gas-phase cluster. The interaction energy, E_{int}, between CO and the cluster is increased by the support effect in all cases, especially for the η_2 mode, where the binding is strengthened by up to 1.2 eV. But for the η_1 mode, this gain in E_{int} is not compensated for by the cost in deformation energy for the substrate. Finally, the support effect with respect to isolated clusters remains moderate; in particular, the stability order of the three modes for CO adsorption is not changed.

The interaction energy of the CO/Pd_4 systems with alumina surfaces (E_{MSI}) is increased on CO adsorption, except in the case of the η_3 coordination on Pd_4/hyd(110). This result is coherent with the reduction in the Pd–O distances and the φ angle after CO adsorption, as noted in the previous paragraph.

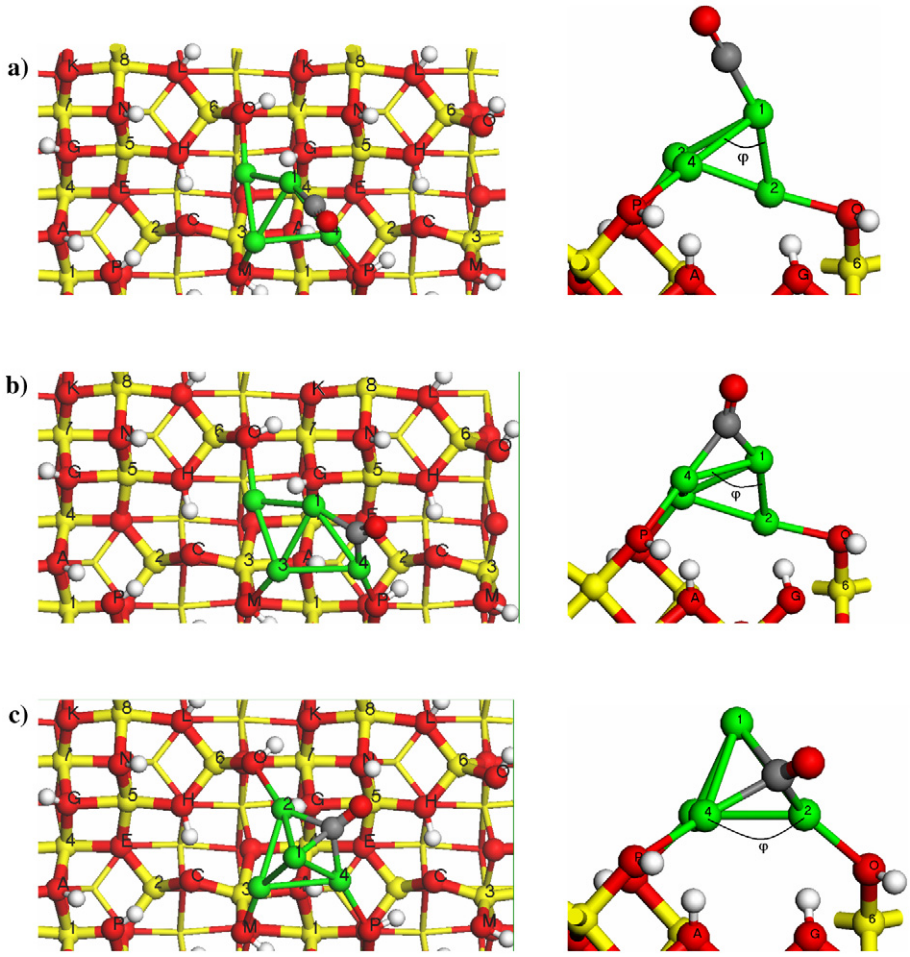

Fig. 4. Top view (left) and side view (right) of the (2 × 1) unit cell of the optimized structures of the CO/Pd_4/Al_2O_3(110) systems: (a) η_1 (top), (b) η_2 (bridge), (c) η_3 (hollow). (Yellow balls: Al, red balls: O, green balls: Pd, small white balls: H, gray balls: C.) (For interpretation of the references to color in this figure legend, the reader is referred to the web version of this article.)

Comparing the (100) and (110) surfaces reveals that the interaction energy of CO/Pd_4 complexes with the support is increased more strongly for the (100) surface. This explains why there is a larger contraction in Pd–O distances on the latter surface. Furthermore, E_{MSI} values are in line with the stronger contraction of Pd–O distances for the η_1 and η_2 modes. In contrast, for the tricoordinated ligand on the (110) surface, the slight expansion found in Pd–O distances is also consistent with the decreased interface interaction energy on CO adsorption. As shown in Table 3, substrate deformation energies are higher on the (100) surface, and, as a result, adsorption energies for CO on Pd_4/γ-Al_2O_3(100) are weaker. In contrast, CO interaction energies with Pd_4/γ-Al_2O_3 (E_{int}) and CO deformation energies do not strongly depend on the support crystallographic orientations. Thus, the difference in adsorption energies between the two support surfaces (0.2 eV) results essentially from the substrate deformation energies.

Interaction energies at the metal–support interface (E_{MSI}) and the shortening of Pd–O bonds shown in Table 1 suggest that the Pd tetramer interaction with the oxide surface is strengthened by CO adsorption. This effect is against intuition, because the formation of new bonds between the cluster and adsorbate would be expected to weaken the interaction between the cluster and support. It clearly suggests a surface and cluster relaxation effect induced by the adsorption process, able to change the structure of the particle–support interface. The results given in this section are similar to those presented previously [36] for smaller Pd_1, Pd_2, or Pd_3 clusters, where a Pd atom is almost inserted in the oxide surface layer. Such a strong interaction mode between cluster and surface is not stable for a Pd_4 cluster but can be achieved when the metallic phase is in interaction with an external adsorbed molecule. Thus, the small deposited cluster is not rigid on CO adsorption. This finding may raise critical issues for the interpretation of infrared (IR) spectra of the CO probe molecule on highly dispersed metal clusters. A strong structural deformation of the metallic phase and the support surface is induced by CO adsorption; therefore, the results of IR spectroscopy of CO for the characterization of small metallic clusters need to be considered with caution.

Another interesting effect of the CO molecule on small metal particles can be suggested. The E_{MSI} values of CO/Pd_4 complexes are significantly higher than those of the Pd tetramer (Table 3), implying that the wetting and morphology of the γ-alumina support by the Pd particles may be enhanced under the

CO gas-phase environment. A similar effect of CO on the shape of Cu particles has been observed by in situ high-resolution transmission electron microscopy for Cu particles supported on ZnO [45], even if the interpretation proposed by Hansen et al. differs slightly from ours. As suggested previously [34], this wetting effect is favored on nonhydroxylated surfaces.

3.1.3. Comparison with ideal Pd surfaces

Even if the comparison between results obtained for the Pd_4 clusters and the numerous published works on Pd surfaces [46–49] is not straightforward, due to the effects of both adsorbate surface coverage and crystallographic orientation, we propose a comparison between our theoretical results and some selected work dealing with the adsorption of CO on Pd(111). E_{ads} values for CO adsorption over Pd(111) at a CO coverage of 1/3 ML are −1.36 for the η_1 mode, −1.81 for the η_2 mode, and −2.01 eV for the η_3 mode of interaction, with a very similar computational approach [46]. These values are significantly lower than those for free and supported Pd tetramers. In particular, on the Pd_4 cluster, the η_3 mode is stabilized by −0.47 eV, and the η_1 mode is stabilized by −0.26 eV. This trend results from the decrease of metal coordination from 9 Pd neighbors on the (111) surface to 3 neighbors for the tetramer. Pd atoms with a lower coordination number clearly develop a stronger interaction with the adsorbate, in a manner congruent with the bond order conservation principle. This effect is not uniform for the different modes, however. The energy difference between the η_2 and η_3 configurations is 0.6 eV for free Pd_4 but only 0.2 eV for the (111) surface. When the Pd_4 cluster is supported on Al_2O_3, the difference between the two modes is again reduced to 0.2 eV, due to increased stabilization of the η_2 mode induced by the support effect.

The size effect on the chemisorption properties of the CO molecule was investigated experimentally by calorimetry measurements. Henry et al. found that the CO chemisorption energy at low coverage increases abruptly from 30 to 40 kcal/mol when the Pd clusters become smaller than 5 nm [50]. Chou and Vannice obtained a similar result for SiO_2-, TiO_2-, and Al_2O_3-supported Pd particles [51]. Although DFT is known to overestimate absolute CO adsorption energies, the calculations reproduce the trend observed experimentally; CO adsorption energies are greater for small Pd_4 clusters with respect to larger systems such as ideal surfaces.

3.2. Adsorption of ethylene

3.2.1. Structural analysis

The structure of ethylene molecules adsorbed on the isolated and supported Pd_4 clusters are presented in Figs. 5–7. The interatomic distances in supported Pd_4 systems are reported in Tables 4 and 5. Two binding modes are possible for ethylene on Pd clusters; in the π mode, a single Pd atom interacts with both carbon atoms, whereas in the di-σ mode, the molecule bridges two neighboring Pd atoms.

Fig. 5 and Tables 4 and 5 show that the C=C bond elongates and Pd–C bonds contract with increasing coordination of the ligand. This behavior may appear to be different than

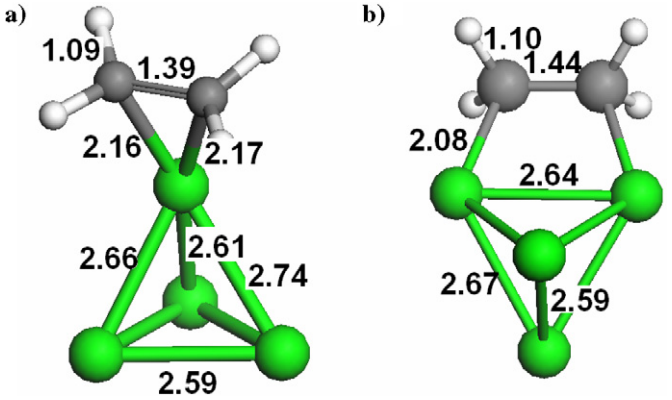

Fig. 5. Optimized structures (distances in Å) of the gas-phase C_2H_4/Pd_4 complexes: (a) π mode ($\theta = 14.8°$ and mean hybridization = 2.27 according to the definition given in the text), (b) di-σ mode ($\theta = 32.9°$ and mean hybridization = 2.60). (Green balls: Pd, gray balls: C, small white balls: H.) (For interpretation of the references to color in this figure legend, the reader is referred to the web version of this article.)

that observed for CO. Nevertheless, in the di-σ configuration, each Pd atom interacts with a single ethylene C atom. Therefore, Pd–C bonds are strengthened as a result of the same bond order conservation mechanism observed for CO adsorbates, whereas a stronger backbonding interaction explains the C=C bond elongation.

On the dehydrated (100) and hydrated (110) surfaces, the average Pd–O distance at the interface is increased slightly after C_2H_4 adsorption, whereas the reverse trend is generally observed for CO [except for the η_3 mode on the (110) surface]. The slight Ir–O elongation after ethene adsorption on Ir_4 clusters supported on γ-Al_2O_3 was also observed by Argo et al. [6]. Adsorption induced rearrangements of the cluster–oxide interface are less pronounced for ethene than for CO; however, this effect is greater for the nonhydrated termination in both cases. In addition, Pd–Pd elongations are slightly less pronounced after C_2H_4 adsorption than after CO adsorption. In all cases, the di-σ mode induces the strongest structural changes (including φ angle distortion). Table 5 reports the θ angle between the bisector direction of the CH_2 unit and the C=C bond direction. This angle, related to the C atom mean hybridization, is equal to 0° for sp^2 hybridization (such as gas-phase ethylene) and 54.7° for sp^3 hybridization (such as gas-phase ethane). The mean hybridization is calculated from a linear interpolation between those two extreme values, assuming hybridization of 2 for $\theta = 0°$ and 3 for $\theta = 54.7°$. According to θ, mean hybridization values, and C=C bond lengths, the ethylene molecule is distorted on adsorption more by supported Pd_4 clusters than by the isolated gas-phase cluster. This result suggests a greater electron transfer from the support to π^* orbitals. Furthermore, the nonhydrated (100) surface induces a slightly stronger perturbation on the mean hybridization than the hydrated (110) surface. A more detailed electronic analysis is reported in Section 3.3.

3.2.2. Energetic analysis

The results in Table 6 show that the π mode of interaction is the most favorable for the isolated Pd_4 ethylene complexes.

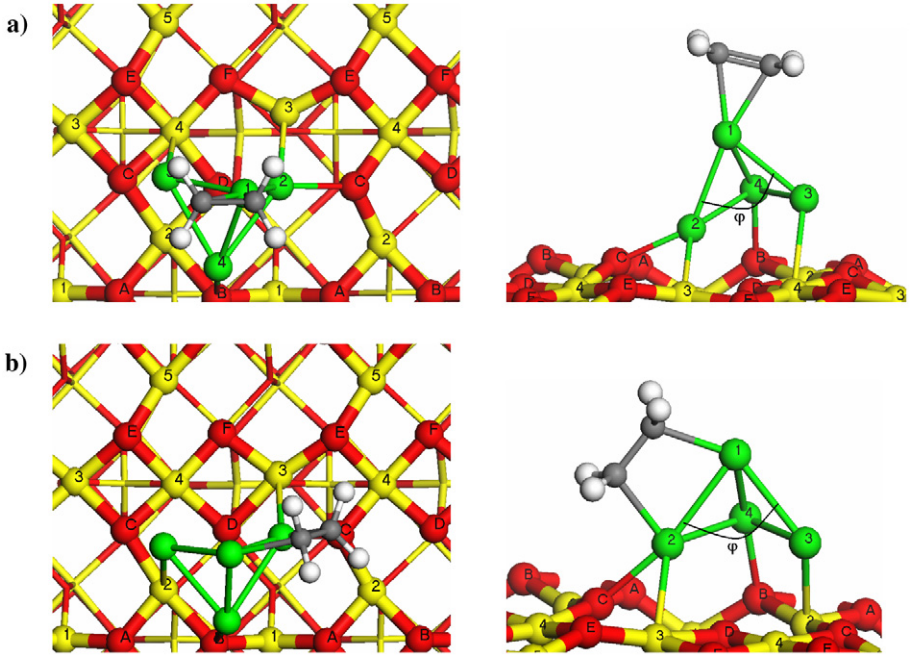

Fig. 6. Top view (left) and side view (right) of the (2 × 1) unit cell of the optimized structures of the $C_2H_4/Pd_4/Al_2O_3(100)$ systems: (a) π mode and (b) di-σ mode. (Yellow balls: Al, red balls: O, green balls: Pd, small white balls: H, gray balls: C.) (For interpretation of the references to color in this figure legend, the reader is referred to the web version of this article.)

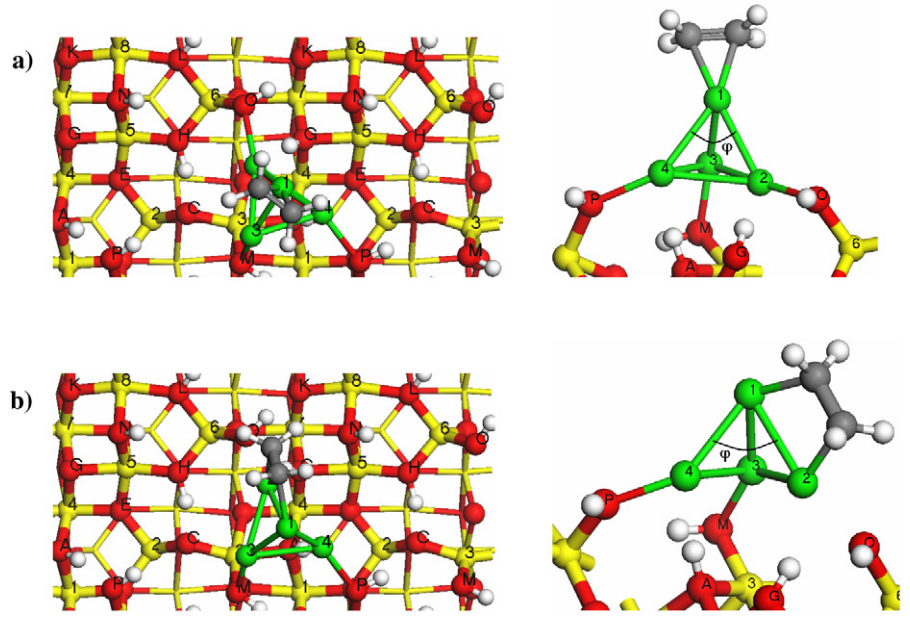

Fig. 7. Top view (left) and side view (right) of the (2 × 1) unit cell of the optimized structures of the $C_2H_4/Pd_4/Al_2O_3(110)$ systems: (a) π mode and (b) di-σ mode. (Yellow balls: Al, red balls: O, green balls: Pd, small white balls: H, gray balls: C.) (For interpretation of the references to color in this figure legend, the reader is referred to the web version of this article.)

Despite a strong increase in ligand–Pd interactions (E_{int}) for the di-σ mode, the π mode remains stable for the hydrated (110) surface. In contrast, the most stable binding site of ethylene is changed to di-σ when the Pd_4 cluster is interacting with the dehydrated (100) surface. The decomposition of adsorption energies into interaction and deformation contributions reveals that the energy spent in substrate deformation on the (100) surface is twice that on the hydrated (110) surface. This explains the overall weaker ethylene adsorption when the cluster is interacting with the dehydrated alumina. However, the cost of this deformation is almost equivalent for the two adsorption modes and thus cannot explain the reversed site preference between the two supports. The difference arises instead from the modified interaction energy. Compared with gas-phase Pd_4, the interaction energy for the di-σ mode is increased by 0.56 eV when the cluster is supported on the dehydrated oxide, whereas the

π mode is destabilized by 0.05 eV. As a result, and because deformation costs are equivalent, the di-σ mode becomes the most stable. In the case of the hydrated (110) oxide support, the differential gain in interaction energy of di-σ versus π mode is only 0.3 eV, and the most stable mode remains π. The modification of the ethylene binding mode due to the nature of the support may has significant consequences on the reactivity of ethylene, because it has been shown that, for example, the π mode is more active for hydrogenation [52,53].

The interaction energies at the metal–support interface (E_{MSI}) are close to or slightly lower than those of the Pd_4 cluster with the support before ethylene adsorption. This trend differs significantly from than seen for the CO molecule and explains why Pd–O bonds contract less on the (100) surface or even elongate on the (110) surface on ethylene adsorption. Consequently, substrate deformation energies are lower on ethylene adsorption compared with those on CO. Comparing the results reported in this section and those for the CO molecule reveals that substrate deformation energies are more important for the (100) surface than for the (110) surface for both ligands; however, in contrast to the CO molecule, these values do not depend on the adsorption mode.

3.2.3. Comparison with ideal Pd surfaces

Numerous studies also have been devoted to the adsorption of ethylene on Pd surfaces [53–56]. The calculated adsorption energies for C_2H_4 over Pd(111) at a coverage of 1/4 ML are -0.62 for the π mode and -0.81 eV for the di-σ mode [54]. The latter mode of interaction is clearly the most favorable on this metal surface. The same result was found for the more open (110) surface (where the Pd coordination is 7), with a lower energy difference of 0.14 eV [53,54]. The energetic trend for C_2H_4 adsorption over a metal surface was correlated with the metallic coordination number, due to a reduced Pauli repulsion between ethylene-occupied molecular orbitals and the surface bands in sites with low metal coordination, as shown qualitatively previously [55]. According to that work, π modes of interaction are favorable for sites with coordination below 7. This is consistent with our calculations for isolated Pd_4 clusters, where the very low coordination number of Pd stabilizes the π mode.

For supported Pd_4 clusters, the stability of the π and di-σ modes depends on the nature of the support. For the (100) surface with strong metal–support interaction energies (E_{MSI}) and strong substrate relaxation energies, the di-σ mode is favored. Therefore, hydroxylation of the Al_2O_3 favors the π mode by reducing the metal–support interaction and substrate relaxation.

3.3. Electronic analysis of the metal–support interactions

We have carried out an electronic analysis of the adsorbed states described previously to improve our understanding of the various trends governing CO and ethylene adsorption on isolated and supported Pd_4 clusters. We analyzed the electronic interactions involved in the molecule–cluster–oxide systems described in the previous section by plotting density of states (DOS) diagrams (with the absolute Fermi level corrected by the value for the electrostatic potential in the vacuum between slabs of the supercell) and electron density difference maps. First, we describe the metal–support interactions in supported Pd_4 clusters before any molecular adsorption; then we analyze how the metal–oxide interface is affected by the incoming ligand (CO or ethylene). Finally, we provide an analysis of the spin ground state.

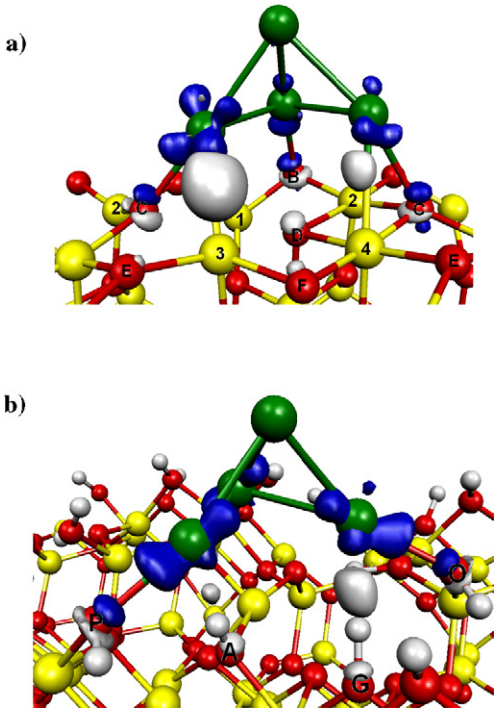

Fig. 8. Maps of electron density difference for γ-Al_2O_3 supported Pd_4 clusters: (a) (100) surface, (b) (110) surface. (Yellow balls: Al, red balls: O, green balls: Pd, small white balls: H, gray balls: C. White lobes: regions of electron density increase. Blue lobes: electron depletion regions. *Note*: For the sake of clarity, label M cannot be visualized in Fig. 8b, the reader can refer to Fig. 11c). (For interpretation of the references to color in this figure legend, the reader is referred to the web version of this article.)

3.3.1. Supported Pd_4 clusters

(100) surface Fig. 8a represents the electron density difference maps for free and supported Pd_4 on the (100) surface. During the adsorption process, polarization of the electron density occurs on surface oxygen atoms. Oxygen atoms in direct interaction with Pd atoms show an electronic depletion in the region between Pd and O, whereas the charge increases in the region between these O atoms and nearby Al atoms. In addition, the corresponding Pd atoms lose electronic charge on *d*-like orbitals on interaction with oxygen. Such a situation, with a charge loss in both orbitals implied in the bond, is characteristic of four-electron interaction to decrease Pauli repulsion. In contrast, charge is accumulated at the Pd–Al bond center, a region of overlap between *s*–*p* hybrid orbitals on Pd and Al, forming a Pd–Al bond.

The projected DOS are shown in Fig. 9 for both the separated cluster and oxide (b) and the interacting system (a). We select sites Al(3) and O(C) to analyze the metal–support interaction. The sharp peak on the O(C) states before Pd_4 adsorption can be

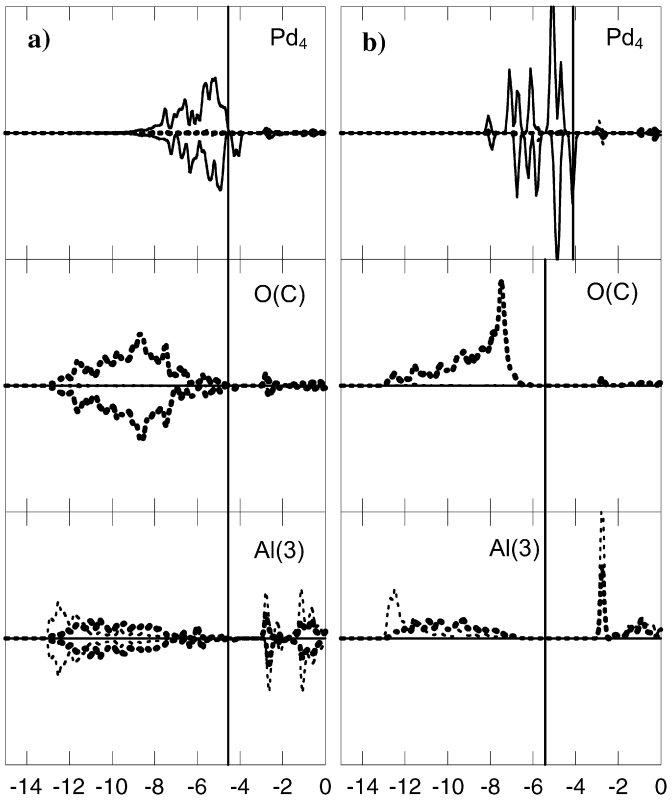

Fig. 9. DOS (arbitrary unit) for the supported Pd_4 cluster on the (100) surface projected on the Pd_4 cluster, $Al_V(3)$ and $O_{III}(C)$ surface sites: (a) after adsorption; (b) before adsorption. (Dotted line: *s* states, dotted bold line: *p* states, solid line: *d* states.)

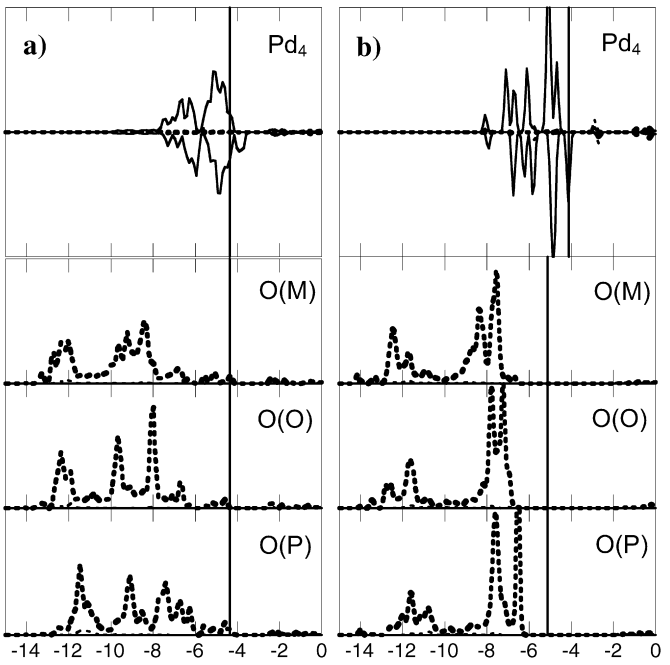

Fig. 10. DOS (arbitrary unit) for supported Pd_4 cluster on the hydrated (110) surface projected on the Pd_4 cluster and O atoms labeled (M), (O) and (P) of three μ_1OH groups: (a) after adsorption; (b) before adsorption. (Dotted bold line: *p* states, solid line: *d* states.)

attributed to a lone pair characterizing the Lewis basicity of the O site [31]. The Al(3) species presents a very localized vacant *sp* state in weak interaction with O(C). This vacant state is the signature of the Lewis acid center [31].

On Pd_4 adsorption, the electronic structure on the surface oxygen and aluminum atoms is modified; the sharp peak of the O(C) lone pair disappears with a marked stabilization of electron states in O(C). New resonances appear in the interval [−8, −4 eV] from mixing with the Pd states on both oxygen and aluminum. As a result, a slight spin polarization appears on these atoms. For the oxygen atom, some antibonding contributions are pushed above the Fermi level, and thus the O(C) atom has more vacant states. This is the origin of the reduced electron density in the direction perpendicular to the surface plane. Another important effect for the O(C) atom is the increased participation in low energy states. This is related to indirect reorganization of surface Al–O bonds and increased electronic density between Al and O atoms (as shown in Fig. 8a). Note that the Al(2)–O(C) and Al(3)–O(C) bonds measure 1.87 and 1.99 Å before Pd_4 adsorption and 1.84 and 2.29 Å after Pd_4 adsorption. We found a similar surface rearrangement in our previous work on the adsorption of Pd single atoms [34].

After adsorption and surface interaction, a broadening of Pd states occurs. This interaction pushes some of the metal *d* states to just above the Fermi level and accounts for the electron loss in these orbitals. As for the Al projected DOS, we note a strong mixing of *sp* orbitals and new contribution from mixing with Pd states in the [−7, −5 eV] region of the diagram. This corresponds to the region in which the electron density difference increases (Fig. 8a). Moreover, there is a small modification in the low energy range from the rearrangement of Al–O bonds.

Hence, the cluster–surface interaction can be summarized as a polarization effect due to a four-electron interaction between states localized in the Pd cluster and O lone pairs in the surface. Some of the metal cluster electrons are pushed above the Fermi level and displaced to previously depleted states localized between Pd and Al atoms. This interaction induces a rearrangement of surface Al–O bonds.

Hydrated (110) surface The map of the electron density difference diagram is presented in Fig. 8b. Fig. 10 depicts the density of states projected on the Pd_4 cluster and on the oxygen atoms of three relevant μ_1OH groups linked to the tetramer. Oxygen lone pairs before Pd_4 adsorption can be easily identified. Oxygen atoms labeled as (O) and (M) are bonded to unsaturated tricoordinated and tetracoordinated Al atoms, respectively, whereas oxygen (P) is bonded to a pentacoordinated Al atom, thus explaining the differences in the DOS; oxygen (M) and (O) develop stronger interaction with Al [34]. This further implies that O(P) exhibits the most basic Lewis character of the three groups of the (110) surface. The absolute energy level of its *sp* state in Fig. 10b appears to be even more basic than that of the O atom of the (100) surface (Fig. 9b). This will have an effect on the donor character of the surface, as described in Section 3.3.2.

Some aspects of Pd_4 adsorption on the hydrated (110) surface are similar to those of the dehydrated (100) termination. The electron density reveals depletion in the Pd–O region be-

tween the Pd base and surface μ_1OH groups linked to the tetramer. The main difference is the nature of the acceptor-type orbitals. The Al atoms are saturated by water, and an increased electron density occurs in the vicinity of some surface O–H groups, such as OH(O), OH(P), OH(G), and OH(A). Thus, we can identify two types of electronic reorganization after cluster adsorption. First, the protons of the OH(G) and OH(A) groups (not directly involved in the Pd–O interaction) have a Lewis acid character and interact with the electron-rich cluster. This can be seen as an additional electronic basin between Pd atoms and the surface OH(G) and OH(A) in Fig. 8b. This first effect is associated with a significant increase of the O–H bond after Pd_4 adsorption (0.2 Å) and a short Pd–H contact (around 2 Å), consistent with a weak Pd–H bond formation. (In a Pd hydride, this distance may vary between 1.67 and 2.02 Å.)

Second, an electron polarization also occurs similar to that seen for the (100) surface. The electron density at oxygen sites in the metal–support interface rearranges in a similar manner: electron depletion in the Pd–O region, between the Pd base and O(O) and O(P) of the μ_1OH groups linked to the tetramer, and an increase in electrons in the O–H bond of those μ_1OH groups. Fig. 10 shows that after Pd_4 adsorption, another important reorganization of the O DOS occurs for the three OH groups involved. The oxygen lone pairs are stabilized to lower energy, congruent with their decreased electronic population.

Moreover, there is a small contribution of oxygen in the vacant states consistent with the electron depletion on these sites described earlier. Finally, Pd *d*-like states are more dispersed and have greater energy after adsorption, consistent with the electron loss seen for those orbitals.

In what follows, we use this information to depict the interaction of these supported clusters with CO and ethylene molecules in an effort to better understand the influence of the support on the chemisorption properties of the cluster and, in turn, the influence of the adsorbates on the cluster–support interaction.

3.3.2. Interaction with CO molecules

Free Pd_4 clusters Identifying contributions from molecular orbitals (MOs) is not straightforward in calculations with a nonlocalized basis set. This was obtained from the *s* and *p* projected DOS and by comparison with standard MO diagrams. On CO adsorption, the 5σ state couples with low-energy Pd_4 cluster states (Fig. 12a.) The Pd_4 projected DOS reveals that the *d* contribution to this state increases with increasing CO coordination to the cluster, with slight energy stabilization. In addition, an antibonding state from the mixing between CO 5σ and cluster *d* states just above the Fermi level can be identified; this is related to the classical picture of four-electron interactions [44]. The $2\pi^*$ orbital mixes with occupied *d* states. This effect is small for the η_1 mode but increases for higher coordinations, suggesting a variation of metal-to-ligand backbonding in the order $\eta_1 < \eta_2 < \eta_3$.

Supported Pd_4 clusters Supported Pd_4 clusters present two major differences with respect to nonsupported metal aggregates. First, the *d* band is broader as a result of the metal–support interaction and delocalization of the electronic *d* states. Second, *d* states are involved in both metal–metal and metal–support interactions. Here we analyze the consequences of these effects on the adsorption of CO molecules. The charge density differences (Fig. 11) and the projected DOS on the CO fragment (Fig. 12) reveal the same qualitative trends on both surfaces with respect to the CO coordination mode, with an increase in backdonation to the $2\pi^*$ CO orbital with increasing metal–ligand coordination. However, there are two major differences with respect to gas-phase CO/Pd_4 clusters. First, the 5σ donation is enhanced in supported systems, and, simultaneously, the $2\pi^*$ band is more dispersed, closer to the Fermi level, characteristic of an increase in backdonation.

Second, there is a strong rearrangement of DOS around the Fermi level. The gap between occupied and unoccupied states is increased with respect to gas-phase CO/Pd_4 complexes, especially for the η_2 configuration and to a lesser extent for the η_3 configuration. This gap opening between occupied and unoccupied states clearly points to a stabilization of CO/Pd_4 complexes by the surface; it is larger for the (100) surface than for the hydrated (110) surface. Therefore, it also may be responsible for the greater stabilization of CO adsorption on the nonhydrated substrate.

The maps of electron density difference for both surfaces and for two adsorption modes (Fig. 11) clearly show the "two-way" electron transfer between CO and Pd atoms, with a 5σ depletion in the CO fragment and a π gain, accompanied by an internal transfer in the *d* orbitals of Pd.

From its interaction with the oxygen atoms of the alumina, the Pd_4 cluster acquires a stronger capability for retrodonation toward $2\pi^*$ states of CO, due to this O (donor)–Pd–CO (acceptor) trans effect. But this effect is valid only for multiple coordination modes of CO. Indeed, for the η_1 mode, backbonding effects are small (due to insufficient overlap between Pd *d* states and $2\pi^*$ of CO), and the interaction is dominated by the donation of the 5σ lone pair to vacant cluster states. CO acts primarily as a donor in η_1 coordination and as an electron acceptor in η_2 and η_3 coordination; thus, the O (donor)–Pd–CO (donor) effect is destabilizing for η_1 coordination. Thus, the support's effect on the chemisorption properties of the particle depends on the synergy between support–particle and particle–adsorbate electron transfers. This explains why CO adsorption energy is decreased in this case of η_1 adsorption of CO and increased for the η_2 mode.

According to the DOS of the (100) and (110) Al_2O_3 surface analyzed in Section 3.3.1, the intrinsic Lewis basicity for the O atom of the μ_1O(P)H group (given by the position of the lone pair sharp peak in the DOS) appears to be strongest of all O atoms involved in the interaction with the Pd_4 cluster. In contrast, the two other O(O) and O(P) atoms exhibit a lower Lewis basicity than the O(C) atom of the (100) surface involved in the interaction (Figs. 9 and 10). This implies that the average electron donor potentiality of both surfaces is rather close, which explains why the resulting interaction energies of CO are sim-

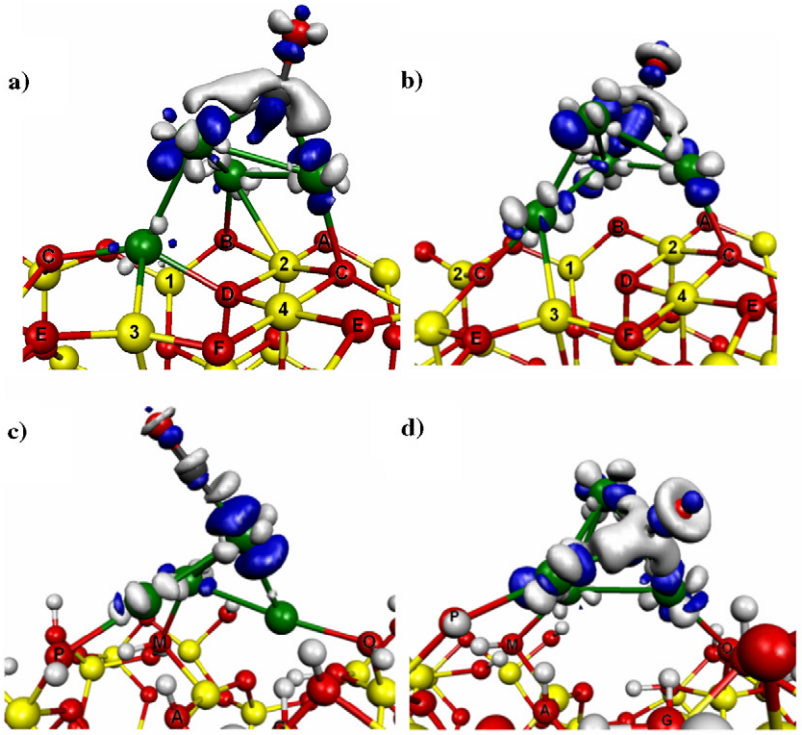

Fig. 11. Maps of electron density difference for γ-Al_2O_3-supported CO/Pd_4 complexes (calculated as the difference between CO/Pd_4/Al_2O_3 and isolated CO and isolated Pd_4/Al_2O_3 with frozen structures): (a) η_1 mode on Pd_4/Al_2O_3(100), (b) η_3 mode on Pd_4/Al_2O_3(100), (c) η_1–CO on Pd_4/Al_2O_3(110), (d) η_3–CO on Pd_4/Al_2O_3(110). (Yellow balls: Al, red balls: O, green balls: Pd, small white balls: H, gray balls: C. White lobes: regions of electron increase. Blue lobes: electron depletion regions.) (For interpretation of the references to color in this figure legend, the reader is referred to the web version of this article.)

ilar. However, because the OH groups have greater flexibility, the deformation energy cost of the substrate is lower, which explains the resulting greater CO adsorption energies on the (110) surface.

3.3.3. Interaction with C_2H_4 molecules

Free Pd_4 clusters The π orbital in gas-phase ethylene overlaps with Pd_4 low-energy states, giving rise to a four-electron interaction analogous to that previously described for CO systems. However, when electrons from the π orbital are transferred to acceptor states localized on another molecule or surface sites, the C=C bond is weakened and the energy of the π^* drops, thus increasing backbonding.

In the π coordination mode, mixing of the ethylene π orbital with Pd_4 low-energy states gives rise to a series of states above the Fermi level, whereas the π^* states decreases in energy and are mixed with vacant *d* states of Pd. As for the di-σ mode, the π orbitals have greater overlap with Pd states, which increases the Pd–ethylene interaction. In addition, an increase in *sp* hybridization occurs, accounting for the higher hybridization index reported in Fig. 5. Combined with the strong increase in ethylene deformation energy due to a change from the π mode to the di-σ mode (Table 6), this suggests that backdonation is enhanced for the latter compound.

Supported Pd_4 clusters The electron difference maps presented in Fig. 13 suggest that electrons previously engaged in Pd–surface bonds have been transferred to the Pd_4/C_2H_4 fragment. Even if quantitatively evaluating the extent to which backbonding is affected by the surface is difficult from our DOS calculations, Fig. 14 also reveals that the interaction of ethylene with γ-alumina–supported Pd_4 affects electronic states involved in bonds at the metal–support interface. This is especially true for the (100) orientation, where occupied states involved in the Pd–Al(3) and Pd–O(C) interaction just below the Fermi level disappear on ethylene adsorption in the di-σ mode. Simultaneously, vacant electronic states of O(C) and Al(3) just above the Fermi level mix with the C–π states for both adsorption modes. This indicates electronic delocalization between adsorbate and support. However, no large gap opening between occupied and unoccupied states as occurs for CO systems is observed, explaining why the support stabilization effect is smaller on ethylene adsorption. Consequently, the O–Pd–C_2H_4 trans effect is significantly weakened with respect to the CO case, due to the lower acceptor character of ethylene in the π mode, which is destabilized on the (100) surface. In the di-σ mode, the acceptor character of ethylene is enhanced, which induces the stabilization of this mode on the (100) surface. This is congruent with the opening of a small energy gap at the Fermi level in this case.

3.3.4. Spin polarization effects

The general consequence of ligands on a magnetic metal cluster such as Pd_4 is to quench the magnetism, by favoring configurations in which spins are paired. However, to reach a stable singlet state, the ligand–cluster interaction must be of a certain strength. For a gas-phase Pd_4 cluster, this is achieved only for CO in the η_2 and η_3 modes, not for the more weakly

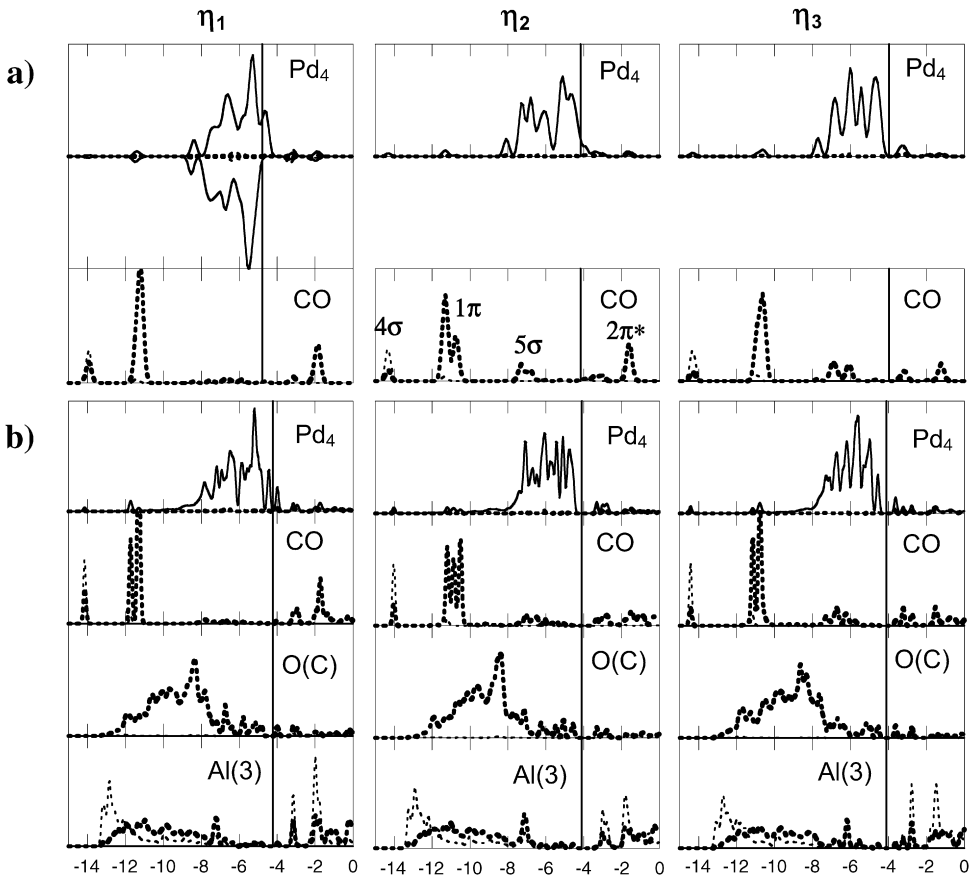

Fig. 12. DOS (arbitrary unit) projected on Pd_4, CO, atoms O(C), and Al(3) for (a) the isolated CO/Pd_4 complex and (b) the (100) γ-Al_2O_3-supported CO/Pd_4 complexes. The η_1, η_2, and η_3 adsorption modes are reported in column 1, 2, and 3, respectively. (Dotted line: *s* states, dotted bold line: *p* states, solid line: *d* states.)

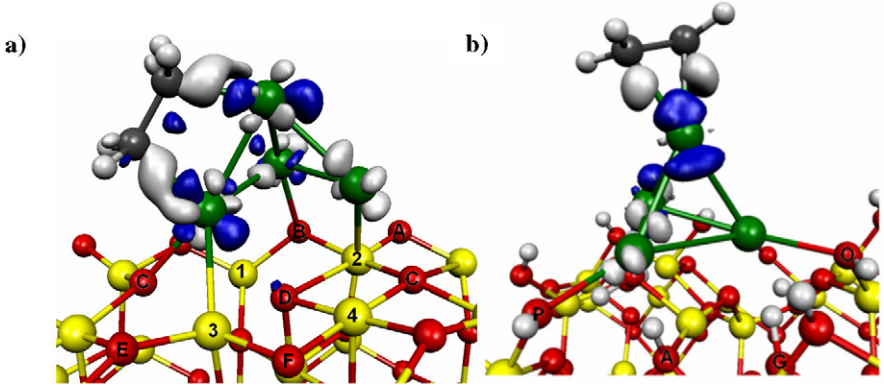

Fig. 13. Maps of electron density difference for γ-Al_2O_3-supported C_2H_4/Pd_4 complexes (calculated as the difference between $C_2H_4/Pd_4/Al_2O_3$ and isolated CO and isolated Pd_4/Al_2O_3 with frozen structures): (a) di-σ mode on $Pd_4/Al_2O_3(100)$, (b) π mode on $Pd_4/Al_2O_3(110)$. (Yellow balls: Al, red balls: O, green balls: Pd, small white balls: H, gray balls: C. White lobes: regions of electron density increase. Blue lobes: electron depletion regions.) (For interpretation of the references to color in this figure legend, the reader is referred to the web version of this article.)

bound η_1, in which a triplet state is retained. Similarly, the cluster–support interaction is not strong enough, and the deposited cluster remains in the triplet state. However, when the surface and ligand effects combine, the CO adsorption on the deposited cluster always yields the singlet state, even for the η_1 mode. The energy differences between the singlet and triplet states are also reported in Table 3.

In contrast, ethylene adsorption is not strong enough to stabilize the singlet state on the gas-phase cluster, and the triplet spin state remains stable whatever the adsorption mode on isolated Pd_4 [57]. If Pd_4 is adsorbed on the support, then the combined ligand effect of the surface and ethylene yields a favored singlet state for the particle. Furthermore, for the di-σ mode of ethylene, the singlet state on Pd_4 is more strongly stabilized on the (100) surface than on the (110) surface. As shown in Table 6, the singlet state is −0.37 eV lower in energy with respect to the triplet on the (100) surface. This can be interpreted as an increased donor character of this surface, resulting in a nar-

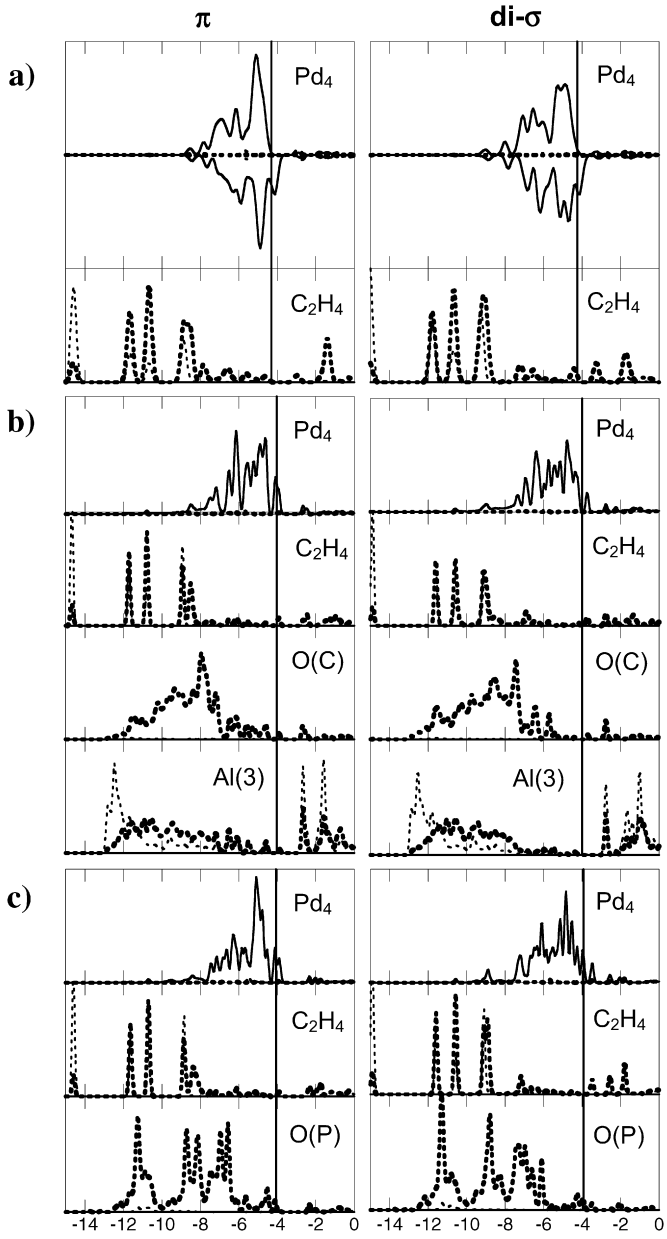

Fig. 14. DOS (arbitrary unit) projected on Pd_4, C_2H_4, atoms O(C), and Al(3) for (a) the isolated C_2H_4/Pd_4 complex, (b) the γ-$Al_2O_3(100)$-supported C_2H_4/Pd_4 complex, (c) the γ-$Al_2O_3(110)$-supported C_2H_4/Pd_4 complex. The π and di-σ modes are reported in column 1 and 2, respectively. (Dotted line: *s* states, dotted bold line: *p* states, solid line: *d* states.)

row gap opening at the Fermi level (Fig. 14b), as mentioned earlier. On the hydroxylated (110) surface, the singlet state is stabilized by only −0.17 eV with a zero density DOS of states at the Fermi level (Fig. 14c).

4. Conclusion

In this work, we analyzed the adsorption of carbon monoxide and ethylene molecules on free Pd_4 clusters and Pd_4 clusters supported on the nonhydrated (100) and hydrated (110) γ-alumina surfaces. First, a comparison of the results obtained for gas-phase Pd_4 cluster and an infinite Pd(111) surface (model of large Pd particle sizes) reported in the literature confirms that adsorption energies are increased for the isolated cluster. This is a consequence of the low coordination number of Pd atoms in the cluster. Furthermore, in contrast to the infinite surface (or large particles), the π adsorption mode of C_2H_4 is stabilized versus the di-σ mode for Pd_4 clusters due to a decrease in the Pauli repulsion in low-coordinated Pd_4.

However, the γ-alumina support plays a key role in changing the qualitative and quantitative trend for the adsorption of the CO and C_2H_4 molecules on Pd_4 clusters. To enhance the adsorption of these molecules, the Pd_4 clusters are deformed to optimize its interaction with the alumina support, giving rise to strong deformation energies. In particular, for the CO molecule, the calculations reveal that Pd_4–CO interactions are strongly counterbalanced by the contribution of substrate deformation energies (with values up to 0.94 eV). In the case of C_2H_4, substrate deformation energies are smaller (up to 0.40 eV) even if they cannot be neglected.

Close inspection of structural parameters, the decomposition scheme of adsorption energies, and the electronic analysis reveal a strong influence of the metal–support interface on the resulting adsorption energy. Both Pd and surface oxygen are polarized on interface formation. For the (100) surface, this implies the formation of Pd–Al bonds and the reorganization of Al–O bonds, leading to the strong substrate deformation energies. In contrast, on the hydrated (110) surface, the electron polarization of O atoms belonging to OH groups implies a charge redistribution concentrated around the latter and thus involving weaker substrate deformation energies. This finding highlights the specific role of hydroxyls on the surface.

The adsorption of CO molecules induces a weakening of the cluster Pd–Pd bonds and a strengthening of the interaction between Pd atoms and surface sites. Moreover, a strong trans effect between the surface O electron donor groups and the electron acceptor CO molecule is seen for the η_2 and η_3 adsorption modes. This results in a counterintuitive increase of cluster–oxide interaction on CO adsorption. As a consequence, supported Pd_4 clusters are chemical species with specific properties different from those of both free Pd_4 and infinite Pd surfaces. Due to this strong metal–support interaction energy for CO/Pd_4 complexes, it has been suggested that the shape and wetting of small Pd particles can change under CO. In contrast, the adsorption of ethylene molecules, which have a stronger electron donor character, cannot present such synergy in electron transfer with the surface, especially for the η_1 mode. As a result, the metal–support interaction is weakened on adsorption.

Our results demonstrate that the two surfaces of the γ-Al_2O_3 support behave differently on adsorption of an incoming ligand. Indeed, Pd–ligand interactions affect electronic states at the Pd_4/γ-$Al_2O_3(100)$ interface, whereas the $Pd_4/Al_2O_3(110)$ interface is less perturbed by the presence of an adsorbate. In the former surface, this effect results in Pd clusters strongly interacting with the oxide, as already shown for low-metal coverage Pd monomers, Pd dimers, and linear trimers [34,36]. It is interesting to note that we ruled out the nucleation of Pd trimers in the (100) surface due to the strong deformation induced to the oxide. However, such deformation can be stabilized by the CO

ligand, as our present results show. Therefore, experimenters should be careful when using CO as a probe molecule for IR characterization studies of very small supported Pd clusters.

Finally, our results suggest another interesting surface effect. The stability of CO adsorbed molecules increases in the order $\eta_1 < \eta_2 < \eta_3$ for isolated Pd_4, infinite Pd(111), and supported Pd_4 clusters. However, the adsorption mode of C_2H_4 depends strongly on the coordination number of Pd and can switch from the π mode on isolated Pd_4 and Pd_4/γ-$Al_2O_3(110)$ clusters to the di-σ mode on infinite Pd surfaces and Pd_4/γ-$Al_2O_3(100)$ clusters due to a stronger metal–support interaction and change in the cluster spin state. This finding may offer new insight into the effects of hydroxylation on reactivity in the hydrogenation of olefins for highly dispersed metal particles.

Acknowledgments

The authors thank D. Uzio, C. Thomazeau, and C. Pichon from IFP for fruitful scientific discussions and Dr. Th. De Bruin for the Jaguar calculations undertaken on the C_2H_4/Pd_4 system. M. Corral Valero is grateful to Dr. V. Robert from ENS Lyon and Dr. N. Lorente from Université Paul Sabatier (Toulouse) for their help in electronic analysis, to the IDRIS and CINES supercomputing centers for computer time (Project 950609), and to ANRT-IFP for a research grant.

References

[1] H.-J. Freund, Surf. Sci. 500 (2002) 271.
[2] A.T. Bell, Science 299 (2003) 1688.
[3] C.R. Henry, Surf. Sci. Rep. 31 (1998) 231.
[4] A.M. Argo, J.F. Odzak, B.C. Gates, J. Am. Chem. Soc. 125 (2003) 125.
[5] A.M. Argo, J.F. Odzak, J.F. Goellner, F.S. Lai, F.-S. Xiao, B.C. Gates, J. Phys. Chem. B 110 (2006) 1775.
[6] A.M. Argo, J.F. Odzak, F.S. Lai, B.C. Gates, Nature 415 (2002) 623.
[7] H. Dropsch, M. Baerns, Appl. Catal. A 158 (1997) 163.
[8] K.M. Neyman, N. Rösch, G. Pacchioni, Appl. Catal. A 191 (2000) 3.
[9] L. Giordano, G. Pacchioni, F. Illas, N. Rösch, Surf. Sci. 499 (2002) 73.
[10] A.D. Vitto, L. Giordano, G. Pacchioni, N. Rösch, Surf. Sci. 575 (2005) 103.
[11] P. Euzen, P. Raybaud, X. Krokidis, H. Toulhoat, J.-L. Le Loarer, J.-P. Jolivet, C. Froidefond, in: F. Schüth, K.S.W. Sing, J. Weitkamp (Eds.), Handbook of Porous Solids, vol. 3, Wiley–VCH, Weinheim, 2002, p. 1591.
[12] M. Benkhaled, Thesis, IFP-Université de Poitiers, France, 2004.
[13] M. Benkhaled, S. Morin, Ch. Pichon, C. Thomazeau, C. Verdon, D. Uzio, Appl. Catal. A 312 (2006) 1.
[14] P.L.J. Gunter, J.W.H. Niemantsverdriet, Catal. Sci. Rev. Eng. 39 (1997) 77.
[15] S.A. Nepijko, M. Klimenkov, M. Adelt, H. Kuhlenbeck, R. Schlögl, H.-J. Freund, Langmuir 15 (1999) 5309.
[16] C.R. Henry, Surf. Sci. Rep. 31 (1998) 231.
[17] G. Kresse, M. Schmid, E. Napetschnig, M. Shishkin, L. Köhler, P. Varga, Science 308 (2005) 1440.
[18] M. Frank, R. Kuhnemuth, M. Bäumer, H.J. Freund, Surf. Sci. 454 (2000) 968.
[19] V. Matolin, I. Stara, N. Tsud, V. Johanek, Prog. Surf. Sci. 67 (2001) 167.
[20] A. Guerroro-Ruiz, S. Yang, Q. Xin, A. Maroto-Valiente, M. Benito-Gonzalez, I. Rodriguez-Ramos, Langmuir 16 (2000) 8100.
[21] T. Lear, R. Marshall, J.A. Lopez-Sanchez, S.D. Jackson, T.M. Klapôtke, M. Bâumer, G. Rupprechter, H.J. Freund, D. Lennon, J. Chem. Phys. 123 (2005) 174706.
[22] M. Frank, M. Bäumer, Phys. Chem. Chem. Phys. 2 (2000) 3723.
[23] H.-J. Freund, M. Bäumer, J. Libuda, T. Risse, G. Rupprechter, S. Shaikutdinov, J. Catal. 216 (2003) 223.
[24] Sh. Shaikhutdinov, M. Heemeier, M. Bäumer, T. Lear, D. Lennon, R.J. Oldman, S.D. Jackson, H.-J. Freund, J. Catal. 200 (2001) 330.
[25] A.M. Doyle, S.K. Shaikhutdinov, S.D. Jackson, H.J. Freund, Angew. Chem. Int. Ed. 42 (2003) 5240.
[26] X. Krokidis, P. Raybaud, A.E. Gobichon, B. Rebours, P. Euzen, H. Toulhoat, J. Phys. Chem. B 105 (2001) 5121.
[27] C. Wolverton, K.C. Hass, Phys. Rev. B 63 (2000) 24102.
[28] G. Paglia, A.L. Rohl, C.E. Buckley, J.D. Gale, Phys. Rev. B 71 (2005) 224115.
[29] G. Paglia, C.E. Buckley, A.L. Rohl, B.A. Hunter, R.D. Hart, J.V. Hanna, L.T. Byrne, Phys. Rev. B 68 (2003) 144110.
[30] M. Digne, P. Sautet, P. Raybaud, P. Euzen, H. Toulhoat, J. Catal. 211 (2002) 1.
[31] M. Digne, P. Sautet, P. Raybaud, P. Euzen, H. Toulhoat, J. Catal. 226 (2004) 54.
[32] M. Heemeier, M. Frank, J. Libuda, K. Wolter, H. Kuhlenbeck, M. Bäumer, H.J. Freund, Catal. Lett. 68 (2000) 19.
[33] J. Libuda, M. Frank, A. Sandell, S. Andersson, P.A. Bruhwiler, M. Bäumer, N. Martensson, H.J. Freund, Surf. Sci. 384 (1997) 106.
[34] M.C. Valero, P. Raybaud, P. Sautet, J. Phys. Chem. B 110 (2006) 1759.
[35] M.C. Valero, M. Digne, P. Sautet, P. Raybaud, Oil Gas Sci. Technol. 61 (2006) 535.
[36] M.C. Valero, P. Raybaud, P. Sautet, Phys. Rev. B 75 (2007) 045427.
[37] J.P. Perdew, J.A. Cevary, S.H. Vosko, K.A. Jackson, M.R. Pederson, D.J. Singh, C. Fiolhais, Phys. Rev. B 46 (1992) 6671.
[38] J.P. Perdew, Y. Wang, Phys. Rev. B 45 (1992) 13244.
[39] G. Kresse, J. Joubert, Phys. Rev. B 59 (1999) 1758.
[40] G. Kresse, J. Furthmüller, Comput. Mater. Sci. 6 (1996) 15.
[41] G. Kresse, J. Furthmüller, Phys. Rev. B 54 (1996) 11169.
[42] T. Futschek, M. Marsman, J. Hafner, J. Phys. Condens. Matter 17 (2005) 5927.
[43] G. Valerio, H. Toulhoat, J. Phys. Chem. 100 (1996) 10827.
[44] R. Hoffmann, Rev. Mod. Phys. 60 (1988) 601.
[45] P.L. Hansen, J.B. Wagner, S. Helveg, J.R. Rostrup-Nielsen, B.S. Clausen, H. Topsoe, Science 295 (2002) 2053.
[46] D. Loffreda, D. Simon, P. Sautet, Surf. Sci. 425 (1999) 68.
[47] M.K. Rose, T. Mitsui, J. Dunphy, A. Borg, D.F. Ogletree, M. Salmeron, P. Sautet, Surf. Sci. 512 (2002) 48.
[48] P. Sautet, M.K. Rose, J.C. Dunphy, S. Behler, M. Salmeron, Surf. Sci. 453 (2000) 25.
[49] F. Delbecq, P. Sautet, Phys. Rev. B 59 (1999) 5142.
[50] C.R. Henry, C. Chapon, C. Goyhenex, R. Monot, Surf. Sci. 272 (1992) 283.
[51] P. Chou, A. Vannice, J. Catal. 104 (1987) 17.
[52] M. Neurock, R.A. van Santen, J. Phys. Chem. B 104 (2000) 11127.
[53] J.S. Filhol, D. Simon, P. Sautet, J. Phys. Chem. B 107 (2003) 1604.
[54] Q. Ge, M. Neurock, Chem. Phys. Lett. 358 (2002) 377.
[55] J.-F. Paul, P. Sautet, J. Phys. Chem. 98 (1994) 10906.
[56] F. Mittendorfer, C. Thomazeau, P. Raybaud, H. Toulhoat, J. Phys. Chem. B 107 (2003) 12287.
[57] The result for the di-σ mode on isolated Pd_4 was not clearly solved in the literature so far. Thus, we check our result with a different exchange-correlation functional. Calculation using the Jaguar program (version 6.5, Schrödinger, LLC, New York, 2005) and the B3LYP functional, Lacv3P** (triple zeta quality) basis set for all atoms recovers that the triplet state is favored by 0.10 eV for the di-σ mode of ethylene on the isolated Pd_4 cluster; Th. De Bruin (IFP), personal communication.